ECE 445

SENIOR DESIGN LABORATORY

FINAL REPORT

A Compact Material Modulus Measurement Instrument

Team #1

KONGNING LAI (kl41@illinois.edu)
YUNZHI LU (yunzhil3@illinois.edu)
ZIYI LIN (ziyilin4@illinois.edu)
TIANYU FU (tianyuf3@illinois.edu)

TA: Zheyi Hang

May 16, 2025

Abstract

This report presents the design and implementation of a compact, low-cost system for measuring the elastic modulus of soft materials. Inspired by atomic force microscopy (AFM), the system integrates a motor-driven indentation mechanism, strain gauge sensing, and a real-time graphical interface to automate material characterization. Key components include a precision stepper motor, a 3D-printed cantilever, a Wheatstone bridge with a 24-bit ADC, and an STM32-based control system. A PC-based application performs real-time data acquisition, baseline correction, contact point detection using neural networks, and Young's modulus calculation via Hertz model fitting. Verification with PDMS samples demonstrated reliable performance within 10% error. The system meets all functional requirements and provides an accessible solution for mechanical testing in educational and research settings. It prioritizes ease of use, affordability, and compatibility with large-scale or less delicate samples, making it particularly suitable for teaching, rapid material screening, and applications where nanometer resolution is not required.

Contents

1 Introduction **1**
1.1 Background and Objective 1
1.2 Block Diagram 1
1.3 High-Level Requirement List 2

2 Design **3**
2.1 Design Procedure 3
2.2 Design Details 4
2.2.1 Physical Diagram 4
2.2.2 Block Design 4
2.2.3 Tolerance and Risk Analysis 10

3 Verification **12**
3.1 Complete System Verification 12
3.2 Mechanical Module 13
3.3 Electrical Module 14
3.4 Embedded Control Module 15
3.5 Application Software Module 16

4 Costs **18**

5 Schedule **19**

6 Conclusions **20**
6.1 Accomplishments 20
6.2 Uncertainties and Future Work 20
6.3 Ethical Considerations 20

References **21**

Appendix A Example Appendix **22**

1 Introduction

1.1 Background and Objective

Soft materials, such as hydrogels and polymers, play a crucial role in various applications, including biomedicine [1], soft robots [2], and wearable devices [3]. Accurate mechanical characterization of these materials is essential for their effective design and implementation. However, current measurement systems face significant challenges in balancing precision, cost-efficiency, and ease of use, especially for macro-scale testing or rapid screening purposes. On the other hand, a strain gauge-based Wheatstone bridge is applied in a sensing system. The zero shift of the Wheatstone bridge and the Johnson–Nyquist noise of the resistors may lead to measurement inaccuracy. Electromagnetic Interference will also generate significant noise. Since the circuit will integrate ADC, the reflection of a magnetic wave of the transmission line may lead to Bit Error Rate. Since measurements always involve errors, multiple measurements are necessary. Manually performing repeated measurements, collecting data, and analyzing results is a tedious task. A user-friendly graphical control and data analysis software will significantly improve efficiency.

The project will develop a macro-scale instrument replicating the functionality of an atomic force microscope (AFM) for measuring the mechanical modulus of soft materials [4]. The mechanical design will feature a precision-controlled indentation system, consisting of a motor-driven lead screw and a specially designed cantilever attached with a spherical probe. At the same time, the circuit should develop a low-power EMI reduction system that provides extremely accurate measurements. The circuit will optimize the routing of the PCB to eliminate reflection. A good software system can also reduce the measurement iterations as the software features a user-friendly interface that allows users to perform measurements through simple buttons and input fields while displaying the results in real-time. It can correct and analyze data, automatically select the appropriate contact model, and calculate the Young's modulus.

1.2 Block Diagram

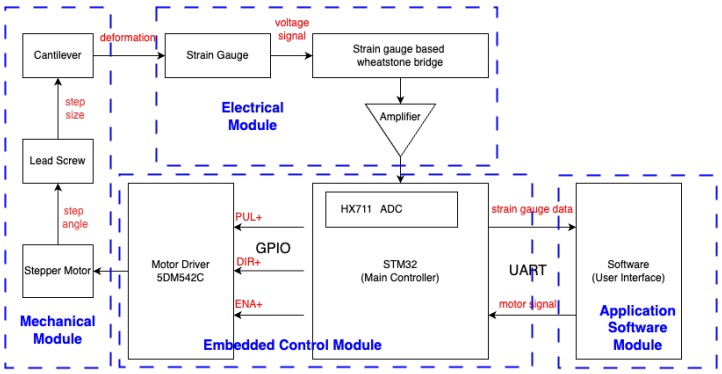

Figure 1: Block Diagram

The overall system structure is illustrated in the block diagram (Figure 1):

- **Mechanical Module:** Stepper motor drives lead screw for linear motion; cantilever applies force to sample.
- **Analog Sensing:** Wheatstone bridge with strain gauge detects resistance change.
- **ADC Module:** HX711 converts analog signal to 24-bit digital; added capacitors reduce ripple.
- **Embedded Control:** STM32 microcontroller handles motor control, data acquisition, and UART communication.
- **Application Software:** GUI initializes system, controls motion, and displays/saves force-displacement data.

1.3 High-Level Requirement List

- The mechanical system shall provide a stable mounting platform and enable precise linear motion with a resolution ≤ 1 μm, while the cantilever shall have a spring constant at least $10\times$ greater than the sample's effective stiffness under quasi-static contact.
- The circuit should enable accurate signal measurement and processing with minimized EMI. The PCB design ensures proper impedance matching to prevent signal reflection and loss. The control system must precisely control the stepper motor with the required resolution.
- The control system must accurately and completely transmit control and data signals between the strain gauge, the upper level software, and the motor driver. The upper-level software must accurately convert the strain gauge signal into force and derive the force-displacement curve based on the stepper motor displacement.

2 Design

2.1 Design Procedure

Based on the design requirements, alternative approaches for each functional block were evaluated. A detailed comparison is provided in Table 1.

Table 1: Comparison of Design Alternatives Across Subsystems

Alternative Design	Chosen Design and Justification
Mechanical Design	
DC Motor Actuation: Low cost and simple control. However, lacks precise position control and requires encoders and feedback loops.	**Stepper Motor Actuation**: Enables accurate open-loop control without encoders. Each pulse produces a fixed step, ensuring millimeter-level descent precision. Matches compact and low-complexity system requirements.
Cantilever Fabrication – CNC Machining: High strength and precision, but expensive and time-consuming. Redesigns require complete re-machining.	**Cantilever Fabrication – 3D Printing**: Allows rapid, low-cost prototyping. Tunable infill enables mechanical property optimization without changing design. Greatly accelerates iteration and testing.
Fixed Sample Platform: Simple structure and easier to fabricate. However, cannot accommodate samples of different thicknesses without redesign.	**Vertically Adjustable Sample Platform**: Allows for varying sample thicknesses by adjusting height, improving adaptability and user convenience without altering structural layout.
Power System	
Shared Supply for Analog and Digital: Simpler wiring, but may introduce noise from digital components into sensitive analog paths, degrading measurement accuracy.	**Separated Analog and Motor Domains**: The analog section is powered by STM32's stable 3.3 V LDO; motor uses a separate 9 V battery. This prevents noise coupling, enhances stability, and protects precision signal acquisition.
Data Acquisition	
STM32 Onboard ADC: Convenient and low-cost but limited in resolution and lacks built-in amplification, necessitating external circuitry for small signal measurement.	**HX711 24-bit ADC**: Provides high precision and integrated amplifier tailored for strain gauges. Reduces component count and improves measurement accuracy.
User Interface (UI)	
Standalone LCD or Embedded Touchscreen: Increases system cost and hardware complexity; offers limited UI scalability and interactivity.	**PC-Based with Qt**: Uses existing PC hardware, reducing cost. Qt facilitates UI development and provides responsive interaction and real-time feedback via UART/USB. Improves user experience and debugging.

2.2 Design Details

2.2.1 Physical Diagram

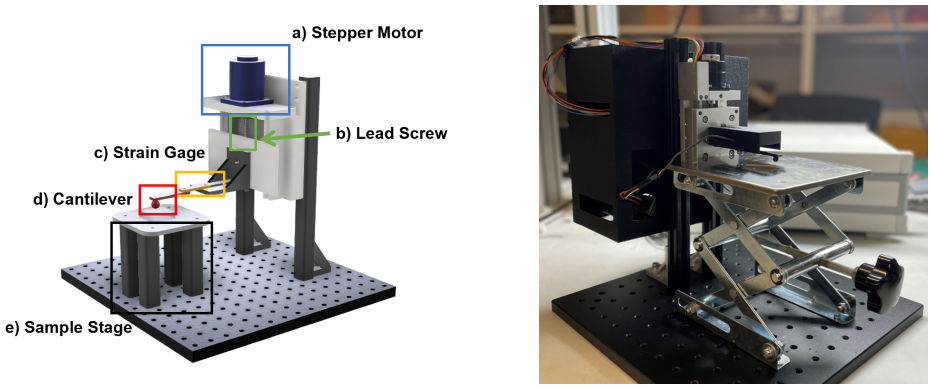

(a) CAD model (b) Final Assembly

Figure 2: Overall System Assembly

In Figure 2a, the system consists of five main components. The stepper motor, mounted high on the bracket with four screws, connects to the lead screw via a flexible coupling to convert rotational motion into linear motion. A 3D-printed sphere at the cantilever tip contacts the sample, inducing bending, which is detected by a strain gauge that converts the deformation into voltage signals. The sample platform is supported by four columns for stability. The fully assembled system is shown in Figure 2b. A sectional view is provided in Figure 12 (Appendix), and orthographic views of the cantilever, motor, and platform are shown in Figure 13, Figure 14, and Figure 15.

2.2.2 Block Design

Mechanical Module The mechanical module consists of three main components: the stepper motor, the lead screw, and the cantilever. The system operates by converting rotational motion from the stepper motor into linear displacement through the lead screw, ultimately applying force via the cantilever to interact with the sample.

Stepper Motor and Screw Coupling

The stepper motor is mounted high on the bracket with four screws to allow manual adjustments during setup and connection to the driver. A flexible coupling links the motor to the lead screw, converting rotation into linear motion to drive the selection module.

To achieve sub-micron step resolution, we use a 5-phase motor with a 0.72° step angle—much finer than the typical 1.8° of 4-phase motors. With 10× microstepping and a 2 mm lead screw, the step size is calculated as follows:

$$\text{Step} = \frac{\text{Screw Lead}}{\left(\frac{1\text{ rev}}{\text{Step angle}} \times \text{Subdivision}\right)} = \frac{1\text{ mm}}{\left(\frac{360^\circ}{0.72^\circ} \times 10\right)} = 0.2\ \mu\text{m} \tag{1}$$

Specially Designed Cantilever

A small sphere is integrally fabricated to the front end of the specially designed cantilever via 3D printing. The sphere comes into contact with the sample, applying force to the sample and causing the cantilever to bend.

The spring constant of the cantilever should be much larger than that of the sample:

$$k_c \gg k_s \tag{2}$$

where k_c represents the spring constant of the cantilever, and k_s represents the spring constant of the sample. This is to ensure that the deformation of the cantilever is mainly dominated by the deformation of the measured materials. The spring constant of the cantilever should be 10 times larger than $k_{s,min}$. The following table contains the parameters designed for the cantilever.

Table 2: Different Cantilever Design Parameters

Dimension (mm)	**Length,** l	**Width,** w	**Thickness,** t	**Diameter,** d
Cantilever 1	30	10	3	8
Cantilever 2	40	10	2	8
Cantilever 3	50	8	2	6

Assuming a minimum detectable resistance change of 0.1% ($\Delta R/R \geq 0.001$) and a gauge factor (GF) of 2.0, the corresponding minimum detectable strain is

$$\varepsilon = \frac{\Delta R/R}{\text{GF}} = \frac{0.001}{2.0} = 5 \times 10^{-4} \tag{3}$$

where ε is the strain and GF is the gauge factor.

If the strain gauge is bonded to the cantilever surface, it experiences the same strain, with maximum strain occurring at the fixed end. Under small deflection, the maximum surface strain at the root is given by

$$\varepsilon = \frac{3\delta t}{2L^2} \tag{4}$$

where δ is the tip deflection, t is the beam thickness, and L is the length. Based on the parameters of cantilever 2, the required minimum vertical deflection to reach the detectable strain is 0.178 mm.

The cantilever finite element simulation under 0.1 N (Figure 3) shows a maximum strain of 6.22×10^{-4} and deflection of 0.301 mm, demonstrating the feasibility of our design.

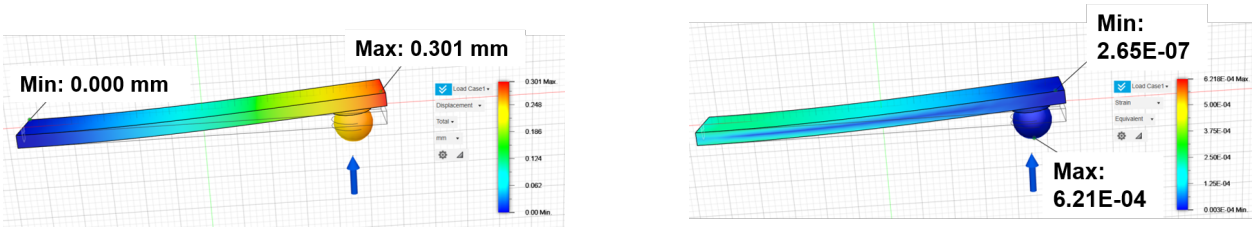

(a) Displacement Simulation (b) Strain Simulation

Figure 3: Finite Element Simulation Results

Electrical Module (analog part) The Wheatstone bridge (Figure 4 left) is used to measure the unknown resistance of the strain gauge. It is constructed using three $220\ \Omega$ resistors, forming a balanced circuit when the gauge is unstressed. Any bending of the gauge leads to a change in its resistance R_x, resulting in a measurable voltage V_g that reflects strain. To enhance the signal-to-noise ratio, the output voltage is amplified by an HX711 amplifier (Figure 4 right), and the amplified signal is then passed to an ADC for digital processing and storage.

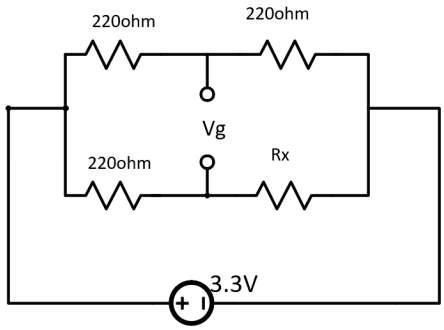

(a) Schematic of the Wheatstone bridge

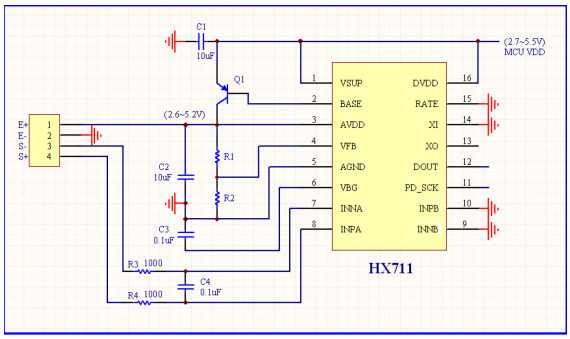

(b) Schematic Overview of the amplifier and ADC

Figure 4: (a) Wheatstone bridge for strain measurement; (b) Amplification and ADC module (HX711)

Analog to Digital Converter and Programmable Gain Amplifier The HX711 is a precision 24-bit ADC specifically designed for applications such as weighing scales and industrial sensors. The amplified signal is fed into the HX711 to generate a digital data stream. Additional capacitors are placed at the analog input node to reduce voltage ripple and ensure signal isolation. The PCB layout (Figure 17) for the HX711 module used in this study is based on Adafruit's open-source design [5]. HX711 is integrated with stm32 on designed pcb board in (Figure 5).

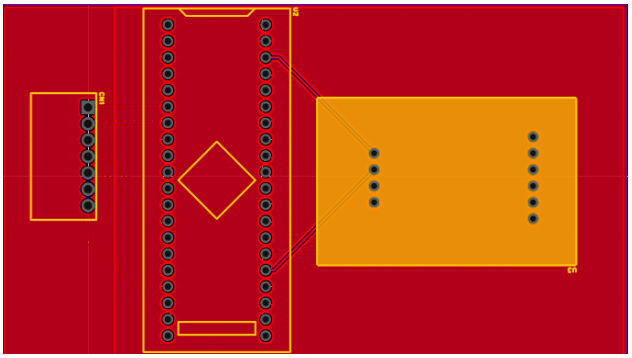

Figure 5: Soldered pcb

Embedded Control Module The Embedded Control Module is responsible for direct motor control, strain gauge data acquisition, and communication with upper-level application software via UART. We use the minimum system board STM32F103C8T6 as the controller, and pin assignment and connection are described in Table 3 and Figure 6:

Table 3: STM32 Pin Assignment Summary

Pin	Function	Description
PB6	TIM4_CH1 (PUL+)	PWM output to control stepper motor pulse signal
PB5	DIR+	Digital output for stepper motor direction control
PB10	HX711 DOUT	Receives strain gauge data from HX711
PB11	HX711 SCK	Clock signal to HX711 (PD_SCK)
PA9	UART TXD	Sends data to PC via CH340 USB-UART
PA10	UART RXD	Receives commands from PC via CH340 USB-UART

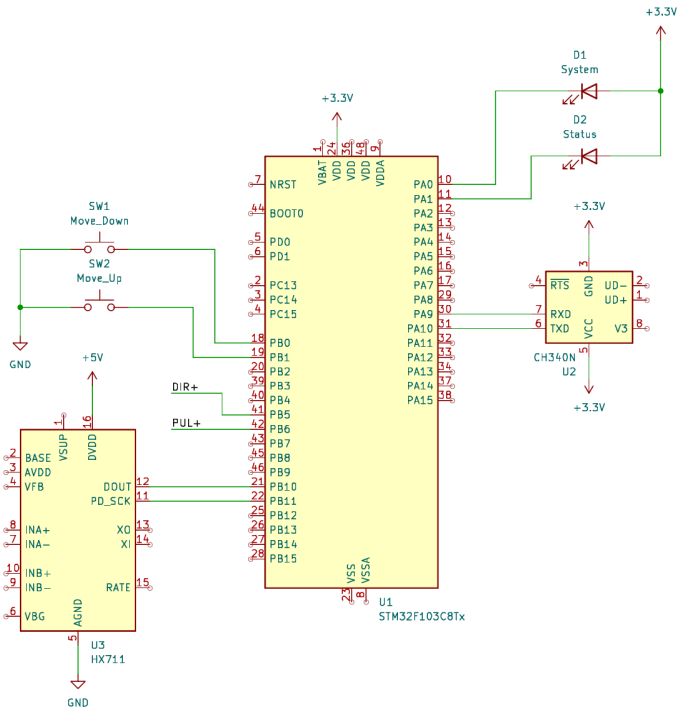

Figure 6: Schematic for STM32 Control System

The control system communicates with the host PC via a serial interface. Upon receiving a START command, the stepper motor initiates forward motion to lower the cantilever, while the HX711 module begins sampling strain gauge data and transmitting it over UART. Contact with the material is determined by detecting a significant change in strain, with noise filtering applied. Once a DIRECTION command is detected, the motor reverses direction and continues moving until a STOP command is received.

Motor Control Module: Timer-Based Stepper Control via GPIO This module controls the stepper motor through the 5DM542C driver using STM32 GPIO pins. The pulse signal for step control is generated via TIM4, while direction and enable signals are handled via dedicated pins. This enables precise displacement control of the cantilever.

Data Acquisition Module: Strain Gauge and HX711 Interface The data acquisition module reads analog strain signals via the HX711 24-bit ADC. The STM32 retrieves digital data via GPIO and transmits it to the PC in real time. This module enables high-resolution force measurements during cantilever-material interaction.

The complete STM32 firmware code for the embedded control system, including motor control, data acquisition, and serial communication, is available at: https://github.com/kongninglai/Compact_Material_Modulus_Measurement_Instrument/tree/master.

Application Software Module This module controls the overall measurement process. It initializes the system, manages user interactions, controls motor movement, and pro-

cesses force-displacement data. The Hertz contact model is used for data analysis [6]. Final results are displayed in the GUI and can be saved to disk. This module consists of three main parts.

Part1. Serial Communication: The serial communication between the STM32 microcontroller and Qt application is handled using the QSerialPort library, configured for 9600 baud rate with 8N1 settings. Port discovery is automatic, scanning available COM ports and populating a dropdown menu. Motor control commands are sent through event-driven button clicks, encoding direction and enable states in hexadecimal. Errors and connection statuses are logged in the message box.

Part2. Data Processing: The conversion from voltage to mechanical measurements uses a calibrated linear model. Masses from 0 g to 50 g in 5g steps are applied to the strain gauge, with sensor readings averaged across three trials. Corrected sensor values are calculated by subtracting the tare value, which is the average of the first 30 readings. A Linear Regression model is fit to the combined data, yielding the transfer function

$$F = (-0.000930 \cdot V + 2.941133) \times 9800 \ \mu\text{N} \tag{5}$$

where V is the raw voltage reading from the strain gauge. Figure 7 shows the linear regression model's fit to the experimental calibration data.

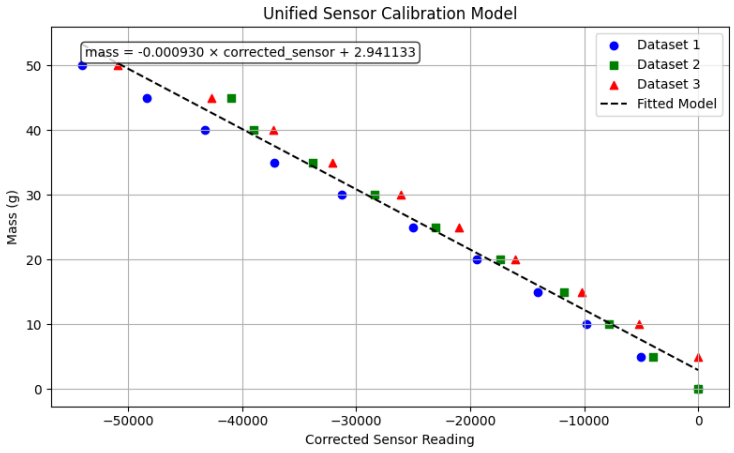

Figure 7: Calibration Curve: The linear relationship between corrected sensor readings and applied mass, based on the derived model.

Displacement calculation leverages the constant motor speed of 0.0325 mm/s, computing position as $t \times 32500$ nm.

The modulus calculation pipeline follows a multi-step analysis process. After collecting and saving the current force-displacement curves, the system first finds the contact point using a convolutional neural network (CNN). This model has two layers with ReLU activation and is trained on 15 samples from 3 different materials, with hand-marked contact points as the reference. Next, the algorithm selects the part of the curve from the peak

force to when the tip leaves the surface, subtracts the contact point offset, and flips it horizontally. For Hertz model fitting, we use an adaptive tip radius method that increases R for softer materials to maintain realistic results. The Hertz model describes the relationship between the applied force and the indentation depth, allowing us to estimate the effective elastic modulus, E_{eff}. We then filter out any results with $R^2 \leq 0.95$ to ensure quality. Here, R^2 (the coefficient of determination) measures how well the fitted curve matches the experimental data. It ranges from 0 to 1, where $R^2 = 1$ indicates a perfect fit, meaning the model explains all the variability in the data. The UI communicates with a Python backend to run this analysis, returning the effective modulus E_{eff} and saving plots that display the raw data alongside the fitted curve.

Part3. User Interface: To achieve a minimum refresh rate of 10 Hz with latency under 200 ms, the module utilizes Qt's signal-slot mechanism to capture incoming data from the serial port. The `receiveInfo()` function appends data to vectors representing time, displacement, and force, which are then visualized on a QChart object. The chart is refreshed dynamically, and axes are adjusted automatically based on the incoming data range.

Motor control is implemented through GUI buttons that trigger serial communication commands. By interacting with buttons for direction and power control, appropriate hex-formatted serial commands are sent to the connected device, ensuring real-time responsiveness.

Data saving and elastic modulus calculation are handled through GUI-triggered functions. Upon clicking the "Save" button, the current F-Z curve data is written to a CSV file, while the "Calculate" button triggers a Python script for elastic modulus computation. Results are parsed and displayed on the GUI for user reference.

2.2.3 Tolerance and Risk Analysis

Tolerance Analysis

The simulation results (Figure 16) indicate that under a vertical load of 0.1 N, the von Mises stress reaches 1.11 MPa. With a safety factor of 15, this confirms that the mechanical structure is sufficiently robust for the intended application. The corresponding simulation figure is provided in the Appendix.

The combination of the stepper motor and lead screw achieves a positional accuracy of 0.01 mm, ensuring precise positioning of the tool or sample. With a repeatability of ± 0.001 mm, the system can consistently perform the same action with minimal error. However, there is a lost motion of 0.003 mm, which introduces small errors during the transmission process, potentially affecting the consistency of force application or displacement.

ADC HX711

The resolution of a 19-bit ADC depends on the reference voltage and the gain setting. For an amplifier with a gain of $G = 128$ and a reference voltage of $V_{\text{ref}} = 3.3\,\text{V}$, the maximum

allowed input voltage is

$$\text{Input}_{\text{allow}} = \frac{V_{\text{ref}}}{\text{Gain}} = \frac{3.3\,\text{V}}{128} \approx 25.78\,\text{mV} \tag{6}$$

Using a 19-bit ADC, the smallest distinguishable voltage step, or resolution, is given by

$$\text{Resolution}_{\text{19-bit}} = \frac{\text{Input}_{\text{allow}}}{2^{19}} = \frac{25.78\,\text{mV}}{524288} \approx 0.049\,\mu\text{V} \tag{7}$$

where G is the gain of the amplifier, V_{ref} is the ADC reference voltage, and $\text{Input}_{\text{allow}}$ is the maximum input signal that can be processed.

Substituting into Equations (6) and (7) gives the final resolution value.

Wheatstone bridge noise simulation @300K

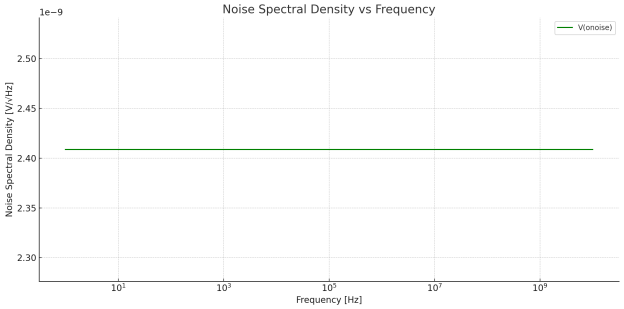

Figure 8: Noise simulation at 300K

the thermal noise Figure 8 for Wheatstone bridge is 2.4 nV, below the detectable range of the ADC, therefore, the thermal noise will not largely affect the circuit output.

Risk Analysis

Mechanical components such as the motor, lead screw, and bearings may degrade over time due to wear, leading to increased backlash and reduced repeatability. Environmental factors like temperature, humidity, and vibrations can also impact performance; for instance, thermal expansion may alter the lead screw or cantilever beam geometry, affecting force accuracy. Regular calibration, the use of high-precision and low-backlash components, and maintaining stable ambient conditions can address these risks.

On the digital side, reliable real-time communication between the Qt interface and STM32 via QSerialPort is crucial. The system must support appropriate baud rates (e.g., 115200 bps or higher), with minimal packet loss (less than 0.5%) and communication latency (under 10 ms) to ensure accurate motor control and sensor feedback.

3 Verification

3.1 Complete System Verification

To verify the complete functionality of our instrument and system, tests were conducted on three different PDMS samples with known elastic moduli. Polydimethylsiloxane (PDMS) is a widely used silicon-based organic polymer, valued for its flexibility, transparency, and biocompatibility. For each PDMS sample, several (no more than ten) sets of experiments were performed using the interface. The interface successfully enabled the extension and retraction of the cantilever by controlling the motor, real-time curve display, data collection and storage, and final result calculation by connecting to Python scripts.

We selected five curves for each material with an R^2 value of at least 0.95 to calculate the average elastic modulus. For each sample, the experimental values were compared against the known reference values. The results showed that the measured values were within an acceptable error range of 10%, satisfying our verification requirements. The scatter dot diagram of the results is shown in Figure 9.

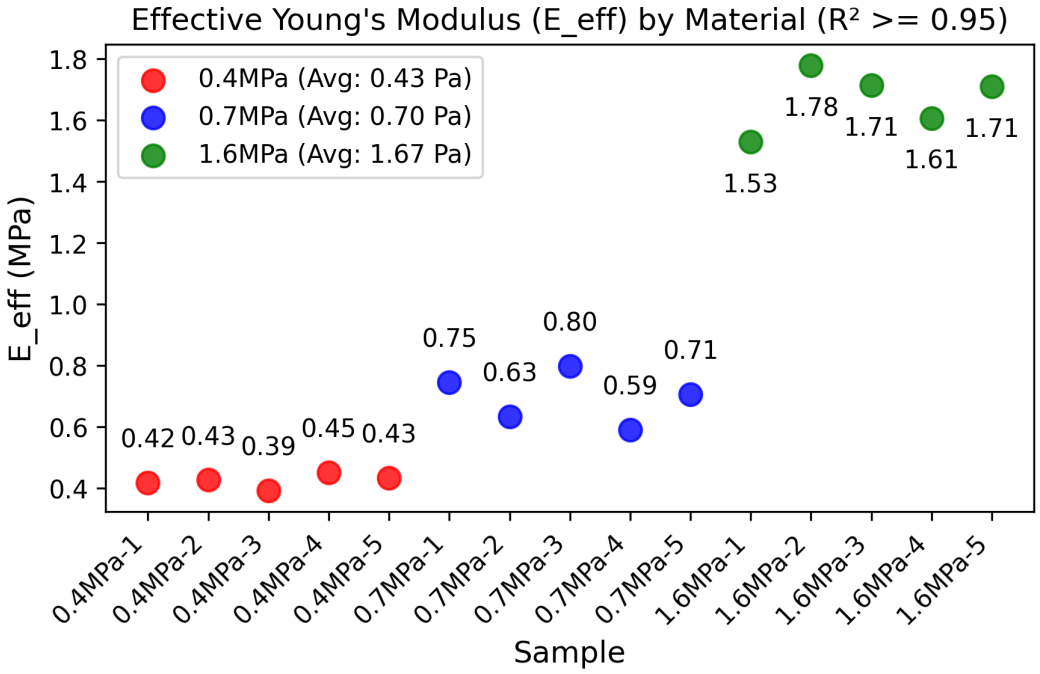

Figure 9: Scatter dot diagram comparing the measured elastic moduli of PDMS samples with known reference values.

However, it is important to note that the PDMS samples used were relatively thin, which required us to stack multiple layers to facilitate measurement. This layered configuration may introduce discrepancies in the modulus calculation due to potential interfacial effects or variations in strain distribution. Another limitation of our current verification process is the lack of additional soft materials with known elastic moduli for further validation. We tested several foam materials with unknown elastic moduli but clear differences in

stiffness. Although the exact values were not known, our measurements accurately reflected the relative differences in hardness. This demonstrates that our system can reliably measure absolute values when available and effectively distinguish relative stiffness in different materials. Therefore, despite the limitations discussed above, the extensive experimental results demonstrate the system's capability to measure elastic moduli accurately and reliably within the specified error range. These findings support the conclusion of our system's overall functionality.

3.2 Mechanical Module

The mechanical verification focuses on the stepper motor-driven screw stage and the cantilever beam. The detailed requirements and verification methods for the mechanical components are summarized in Table 6 (Appendix A). Experimental setups and key verification results are briefly outlined below (10).

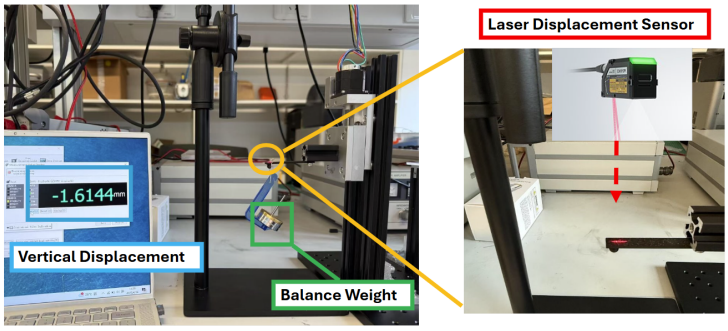

Figure 10: Laser displacement sensor setup used for motor and cantilever testing

Stepper Motor and Screw Stage. To validate the step resolution requirement, the motor was driven with 800, 1600, and 3200 microsteps while the displacement was recorded using a laser sensor (precision 0.1 µm). The average linear displacement was calculated over three repeated measurements.

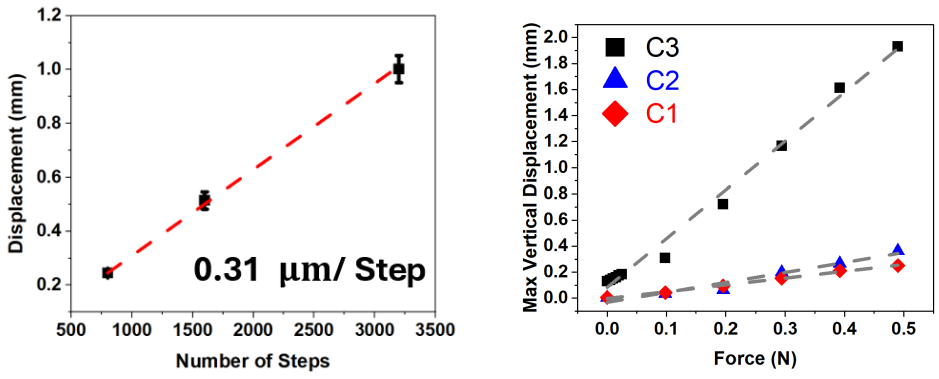

(a) Step resolution test (b) Cantilever deflection under loads

Figure 11: Mechanical module verification results

As shown in Figure 11a, the motor achieved a linear resolution of 0.31 µm per step, well within the required range of 1.0 µm.

Cantilever Beam. The cantilever's spring constant was characterized by applying calibrated weights (1–50 g) and recording tip deflection with the laser sensor. Beam stiffness and deflection under load were calculated using classical beam theory[7]:

$$k = \frac{Ewt^3}{4l^3} \tag{8}$$

where k is the spring constant of the cantilever, E is the Young's modulus of the material, w is the width of the beam, t is the thickness of the beam, l is the length of the beam, and I is the second moment of area.

To ensure measurement precision and sample integrity, the beam was designed to be stiffer than the sample: $k > 10k_s$, where k_s is the estimated stiffness of the sample. Also, to achieve measurable strain levels, the beam was required to deflect at least 0.1 mm under a 0.1 N load.

In Figure 11b, results of three different designs are presented. A full comparison of all cantilever designs (C1–C3) is available in Appendix A, Table 7. For sample C3, the measured spring constant was $k = 267.7$ N/m $> 10k_s = 7.85$ N/m, and deflection under 0.1 N load was 0.31 mm > 0.1 mm, satisfying both requirements.

Potential issues that may affect the accuracy and reliability of the mechanical verification include differences in manufacturing, causing variations in cantilever properties and possible misalignment or calibration errors in the laser displacement sensor setup. Continuous careful characterization and validation will be conducted to ensure robustness and repeatability of the results.

3.3 Electrical Module

Power Supply Verification

Power the bridge using a 3.3 V regulated supply. Use a multimeter or oscilloscope to measure the differential output voltage V_g. Verify that $V_g \approx 0\,\text{V}$ under no load (balanced condition). Apply a calibrated displacement or bending force to the strain gauge. Record the resulting output V_g, and confirm that V_g changes with respect to bending. This confirms the system responds to strain-induced resistance changes.

Wheatstone Bridge Balance Verification The noise floor determines the minimum detectable signal of the system. In strain gauge or bridge-based measurement systems, excessive baseline noise can obscure small signal variations, thus degrading sensitivity and resolution. Verifying the noise level is a key criterion in evaluating the success of the analog front-end design. **Impact of Baseline Noise on Precision:** The baseline noise of the analog front-end directly limits the system's minimum detectable signal (MDS). When the input signal amplitude is lower than the noise floor, it becomes indistinguishable from random fluctuations.

The minimum detectable voltage is bounded by the root-mean-square (RMS) noise:

$$\text{MDS} \geq V_{\text{noise, rms}} = \sqrt{\int_{f_{\text{low}}}^{f_{\text{high}}} S_n(f)\, df} \tag{9}$$

The noise spectral density $S_n(f)$ is flat over the bandwidth Δf, the RMS noise simplifies to:

$$V_{\text{noise, rms}} \approx S_0^{1/2} \cdot \sqrt{\Delta f} \tag{10}$$

$S_0 = (240\ \text{nV}/\sqrt{\text{Hz}})^2$ and $\Delta f = 10$ kHz, the total integrated noise becomes:

$$V_{\text{noise, rms}} = 240\ \text{nV}/\sqrt{\text{Hz}} \times \sqrt{10^4\ \text{Hz}} = 24\ \mu\text{V} \tag{11}$$

Thus, any signal smaller than 24 μV would be buried in the noise and not measurable. This directly limits system resolution and accuracy.

3.4 Embedded Control Module

Motor Control – Stable and accurate motor control

To ensure stable motor control, the frequency of the stepper motor was set to 100 Hz for practical use. For the verification, an oscilloscope was connected to the STM32's motor pulse output pin to check the pulse frequency. The STM32 system clock is set at 72 MHz.

$$f_{PWM} = \frac{f_{system}}{(TIM_period + 1) \times (TIM_prescaler + 1)} \tag{12}$$

Where f_{PWM} is the output PWM frequency, f_{system} is the STM32 system clock (72 MHz), TIM_period is the period register value of the timer, $TIM_prescaler$ is the prescaler register value of the timer.

When TIM4's period is set to 100-1 and the prescaler is set to 7200-1, the output frequency is 100 Hz. Similarly, when the period is set to 100-1 ms and the prescaler is set to 3600-1 ms, the output frequency becomes 200 Hz. These calculated frequencies were measured with the oscilloscope, and the results were found to be exactly 1000 Hz and 2000 Hz, as shown in Figure 18, and Figure 19 located in Appendix A, which is within the required ±2% accuracy.

Motor Control – Direction change within 50 ms of command.

To verify the direction change within 50 ms, Keil's debugging functionality was used to measure the time between receiving a serial direction signal and the output of the GPIO direction change. The clock was synchronized to match the STM32 system clock (72 MHz). By setting breakpoints in the code to mark the moment when the direction signal

was received, and when the direction change code was completed, the time difference was measured across three experiments. The results of the experiments are shown in the Table 8, located in Appendix A.

The average time difference across three experiments was 1.45 μs, which is well within the required 50 ms threshold, indicating that the direction change was correctly implemented and verified.

Data Acquisition – HX711 sample rate $\geq$ 10 Hz, resolution = 24-bit.

The HX711 was configured to output data at a sample rate of 1 kHz, and its 24-bit resolution was confirmed. An oscilloscope was used to observe the SCK (HX711 clock) and DT (HX711 data) outputs. When the DT pin transitioned from high to low, the SCK pin began outputting 24 clock pulses at a frequency of 1 kHz, as shown in Figure 20 located in Appendix A confirming the correct operation of the clock signal and sample timing.

Data Acquisition – HX711 data peak-to-peak noise under static load $\leq$ 1%.

For the verification of peak-to-peak noise under static load, the cantilever was left unloaded, and 100 data samples were recorded. The statistical analysis of the data revealed that the minimum and maximum values were 7352508 and 7355031, respectively. The standard deviation was found to be 531.35, and the mean value was 7353153.18. The noise ratio was calculated as:

$$\text{Noise Percentage} = \frac{531.35}{7353153.18} \times 100 \approx 0.0072\% \tag{13}$$

This result is well within the required limit of less than 1%, demonstrating that the system performs with minimal noise under static conditions.

3.5 Application Software Module

Serial Communication Verification To validate the bidirectional data transmission at a baud rate of 9600, an oscilloscope was connected to the STM32 serial output port (TX) to measure the time interval of the transmitted signal. The measured time difference between signal edges was approximately 104 μs, corresponding to a calculated baud rate of 9615.38 baud. This value is consistent with the target baud rate of 9600, falling within the acceptable 5% margin of error. The oscilloscope interface displaying the measured waveform is shown in Figure 21, located in Appendix A.

We continuously sent data for 60 seconds, saving both the transmitted and received data into separate `.txt` files. Using the `diff` command to compare the two files, we found no discrepancies, indicating that there was no data loss during the transmission. This confirms that the data loss rate is effectively 0%, which meets the requirement of being less than 1%.

Additionally, the system's command processing was validated by transmitting an 8-byte signal to the STM32 using `QSerialPort`. Since the oscilloscope could not measure

the transmission time from the interface, an alternative method was implemented. The STM32 was configured to perform two actions upon receiving the `0x1` command: toggle the GPIO to change the motor direction and return a `0x8` response. On the Qt side, a timer was used to measure the elapsed time from the transmission of `0x1` to the reception of `0x8`. The measured time between sending and receiving the signal on the Qt side was approximately 10 ms, indicating that valid commands triggered correct responses within this 10 ms window, well below the 200 ms requirement.

Data Processing Verification To check the force measurement accuracy, we compared the model's predicted mass values with the actual masses used. The average error was 10.93%, which is higher than the target of 5%. This difference might be caused by noise or calibration problems, especially at lower force levels. To fix this, we could use better signal filtering, improve the calibration process, or adjust the hardware to reduce interference and make the measurements more consistent.

Another requirement about the estimated elastic modulus in this module is verified in the previous subsection 3.1, so it will not be repeated here.

User Interface Verification The real displacement data and corresponding timestamps were analyzed to evaluate the system's performance. First, the refresh intervals were calculated by determining the differences between consecutive timestamps. Subsequently, the refresh rates were obtained as the inverse of these intervals. Finally, the average refresh rate is approximately 10.66 Hz, which satisfies the requirement of 10 Hz. All refresh intervals are consistently under 100 ms, indicating a display latency bounded by the update cycle and data transmission delay. So the latency ≤ 93.75 ms <200 ms, the first requirement of this module is verified.

For the remaining two requirements, we validate them through smooth operation of the UI during the experiments. The **Run/Stop** button effectively starts and stops the motor as expected. The **Direction** functions properly, enabling changes in motor direction with immediate effect.

The interface also supports saving the F-Z curve from the current experiment, with the save path confirmed in the message box. When the **Calculate** button is pressed, the modulus value is correctly computed and displayed in the result box on the UI. Therefore, this module fully satisfies its intended requirements.

4 Costs

As shown in Table 4, the total cost of the project, including estimated labor is approximately 1218.5 RMB, with labor accounting for 10000 RMB based on team effort.

Labor Cost Estimate:
Using the formula:

$$\text{Labor Cost} = \text{Hourly Rate} \times \text{Hours Spent} \times 2.5 \times \text{Team Size} \tag{14}$$

Assuming an hourly rate of 50 RMB/hour, 20 hours per person, and 4 team members:

$$\text{Labor Cost} = 50 \times 20 \times 2.5 \times 4 = \textbf{10000 RMB} \tag{15}$$

Table 4: Bill of Materials for Mechanical and Electronic Components

Name	**Model/Specification**	**Price (RMB)**
Optical Breadboard	300x300x13 M6	252
Strain Gage	350-3AA/120	30
HX711	–	4
Stepper Motor & Screw Stage	VEXTA 5-Phase	495
Stepper Motor Driver	5DM542C	340
STM32 Microcontroller	STM32F103C8T6	34
ADALM1000	–	– (Lab-owned, free)
Aluminum Profile	2020L-1.5 (1 m)	10.9
Manual Lifting Stage	150x150 mm	46.2
Subtotal (Parts)		**1218.5**
Labor Cost (Estimated)		**10000**
Total Cost (Including Labor)		**11218.5**

5 Schedule

The complete timeline of the project is detailed in Table 5. TF = Tianyu Fu, ZL = Ziyi Lin, KL = Kongning Lai, YL = Yunzhi Lu.

Table 5: Project Schedule and Task Allocation

Week	**Task**	**Responsibility**
2/24/25	Initial design discussion	All
3/3/25	Finalize mechanical schematic	TF
	Complete RFA and team contract; Purchase key components	All
3/10/25	CAD modeling (motor, stage, holder)	TF
	Strain gauge test and bridge design	ZL
	Software architecture draft	KL & YL
	PCB assignment and proposal	All
3/17/25	Design 3D-printable cantilevers and start 3D printing	TF
	Develop control submodules	KL & YL
3/24/25	Assemble screw stage	TF
	GPIO control via buttons and via serial	KL
	Improve UI and serial communication	YL
	Start cantilever calibration and test stepper driver V/I	All
3/31/25	Mount motor and holder base	TF
	Test motor driver and linear motion of the cantilever	ZL
	Connect strain gauge + MCU	ZL & KL
	Test ADC and data reading	ZL
	Python scripts for elastic modulus estimation	YL & KL
4/7/25	Refine motion tests	ZL
	Write design document	All
4/14/25	Continue cantilever calibration	ZL
	Data transfer + real-time plotting	YL
4/21/25	Fine-tune motion control	TF
	ML for modulus estimation	KL & YL
4/28/25	Optimize cantilever design	TF
	Integrate Python into Qt	YL
	Full system integration	All
5/5/25	Zero shift and balance tests	All
5/12/25	Final cantilever calibration	All
5/19/25	Analyze results and refine	All
5/26/25	Write final report and Final presentation prep	All

6 Conclusions

6.1 Accomplishments

This project successfully delivers a compact, cost-effective, and precise system for measuring the elastic modulus of soft materials. The mechanical module achieved sub-micron displacement control, while the 3D-printed cantilevers met the desired stiffness and deflection requirements. The analog sensing and data acquisition modules exhibited low noise and high resolution, and the embedded control system provided accurate motor control and reliable communication. The Qt-based software enabled real-time data visualization and automated modulus calculation. Verification tests using PDMS samples demonstrated an error rate within 10%, validating the system's performance and reliability.

6.2 Uncertainties and Future Work

Although the system met design specifications, uncertainties remain. Testing was limited to a small range of soft materials, and the neural network for contact point detection was trained on a small dataset, potentially limiting generalization. Stacking multiple PDMS layers may have introduced interfacial effects affecting modulus estimation. Moreover, since PDMS is a viscoelastic material, the tip speed can influence the measured elastic modulus. We conducted experiments evaluating different pressing speeds. The results (Figure 22) show that the measured elastic modulus increases with higher indentation speeds. Future improvements include adding an infrared displacement sensor for real-time feedback to correct backlash or drift, though this would increase system complexity and cost. A fully automated, one-button workflow could improve usability but would require more sophisticated firmware and event handling. Expanding the training dataset would enhance model robustness, though it would involve additional data collection and labeling efforts. These directions offer pathways to improve precision, automation, and generalizability in future system iterations.

6.3 Ethical Considerations

This project adheres to the IEEE Code of Ethics, emphasizing safety, transparency, and responsible testing. All data was truthfully reported, and team members maintained a collaborative and respectful development environment. The system supports broader access to material testing by offering a low-cost, modular alternative to high-end AFM systems. Its design minimizes environmental impact through 3D-printed components and promotes scientific inclusion in low-resource settings. The device has potential applications in biomedicine, flexible electronics, and material research, contributing positively to global scientific progress and societal well-being.

References

[1] C. Dagdeviren, Y. Shi, P. Joe, *et al.*, "Conformal piezoelectric systems for clinical and experimental characterization of soft tissue biomechanics," *Nature materials*, vol. 14, no. 7, pp. 728–736, 2015.

[2] N. Elango and A. A. M. Faudzi, "A review article: Investigations on soft materials for soft robot manipulations," *The International Journal of Advanced Manufacturing Technology*, vol. 80, pp. 1027–1037, 2015.

[3] H.-R. Lee, C.-C. Kim, and J.-Y. Sun, "Stretchable ionics–a promising candidate for upcoming wearable devices," *Advanced Materials*, vol. 30, no. 42, p. 1 704 403, 2018.

[4] C.-D. Lam and S. Park, "Nanomechanical characterization of soft nanomaterial using atomic force microscopy," *Materials Today Bio*, vol. 31, p. 101 506, 2025.

[5] Adafruit, *Adafruit-hx711-24-bit-adc-pcb: Pcb files for the adafruit hx711 24-bit adc*, https://github.com/adafruit/Adafruit-HX711-24-bit-ADC-PCB/, Accessed: 2025-04-14, 2024.

[6] H. Hertz, "Über die berührung fester elastischer körper.," *J reine und angewandte Mathematik*, vol. 92, p. 156, 1881.

[7] The Engineering ToolBox, *Cantilever beam calculations: Formulas, loads & deflections*, https://www.engineeringtoolbox.com/cantilever-beams-d_1848.html, Accessed: 2025-04-18, 2013.

Appendix A Example Appendix

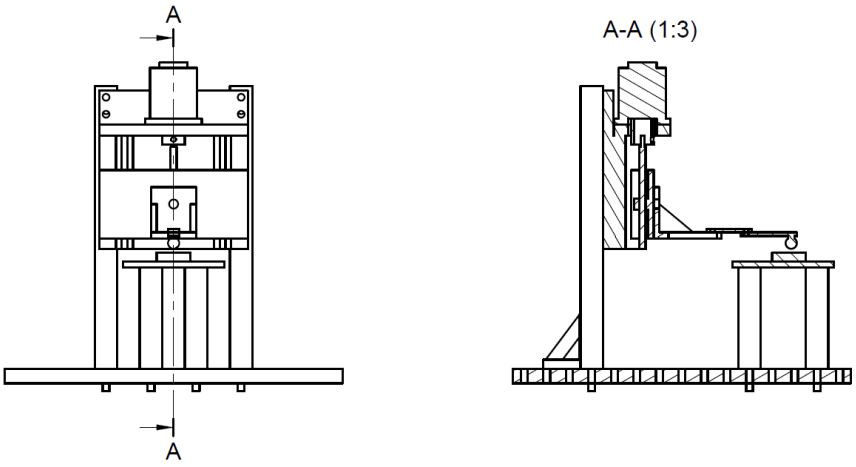

Figure 12: Sectional View

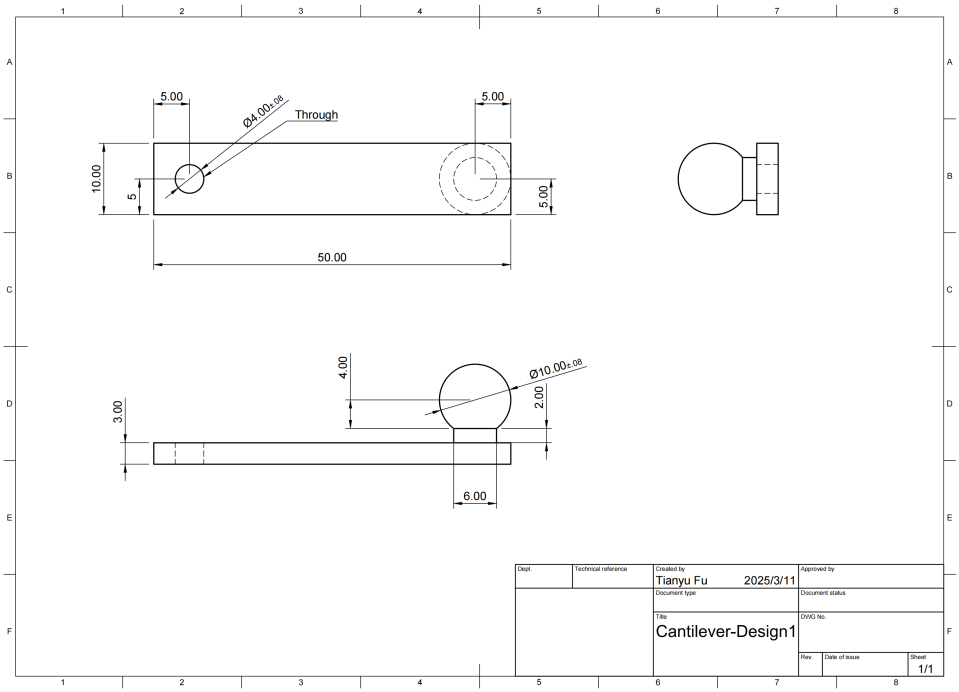

Figure 13: Orthographic Views of the Cantilever

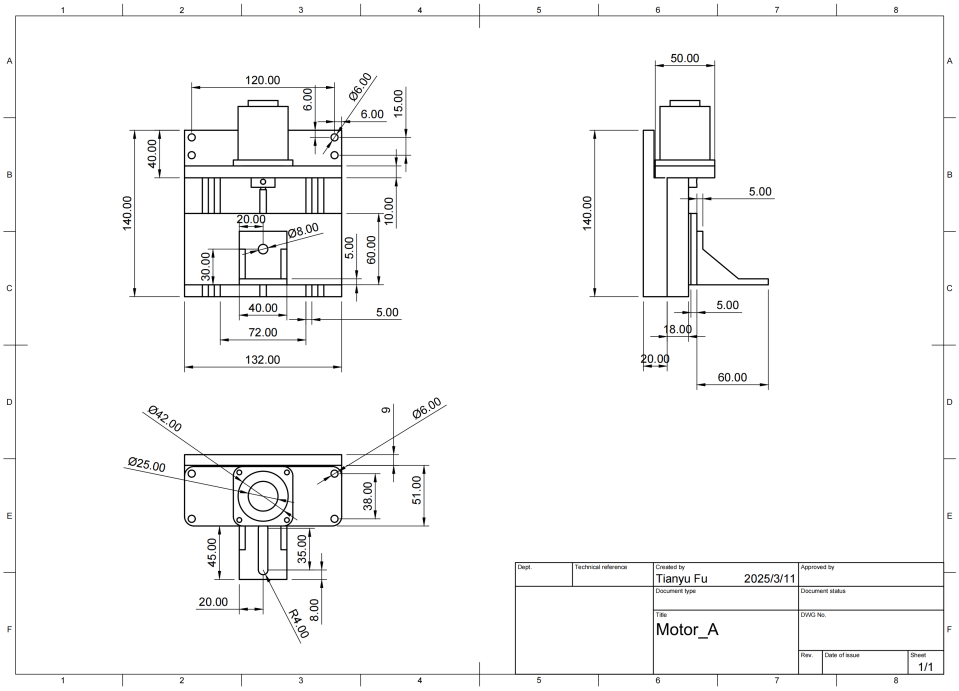

Figure 14: Orthographic Views of the Motor Set

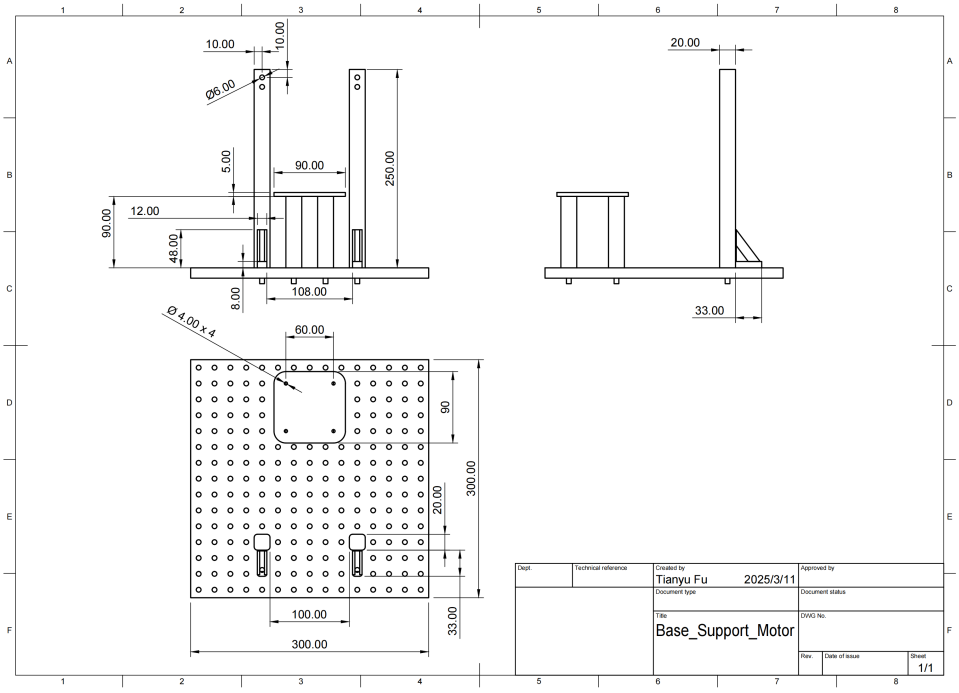

Figure 15: Orthographic Views of the Sample Stage and Supporting Part

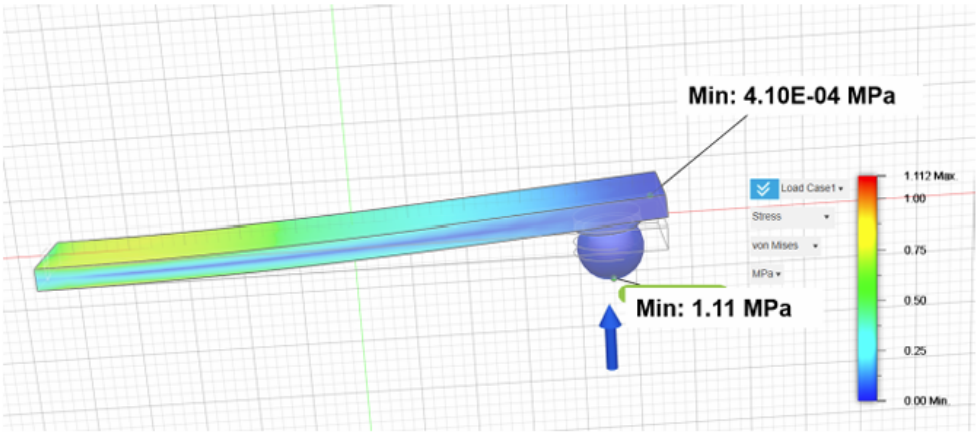

Figure 16: Stress Simulation

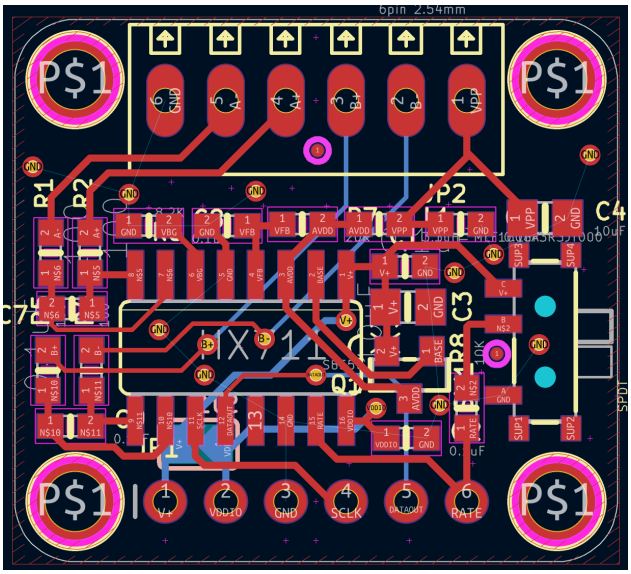

Figure 17: PCB layout

Figure 18: PWM Pulse Frequency 100 Hz

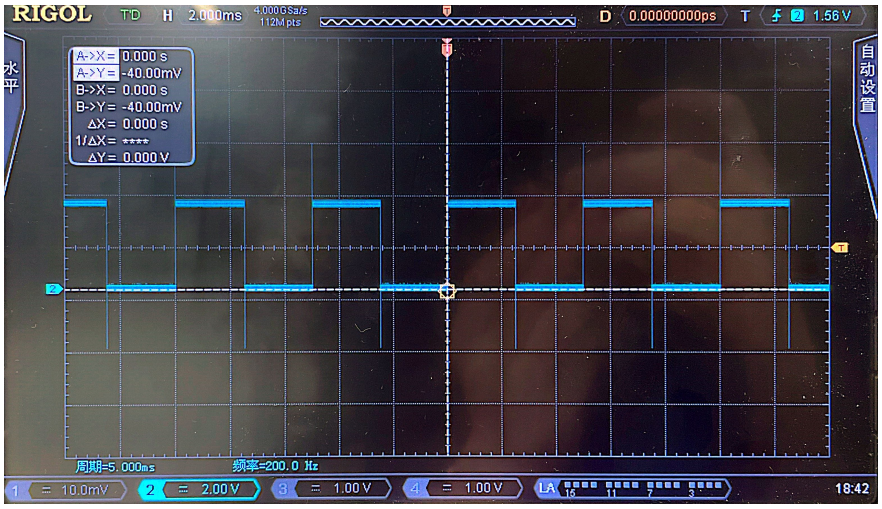

Figure 19: PWM Pulse Frequency 200 Hz

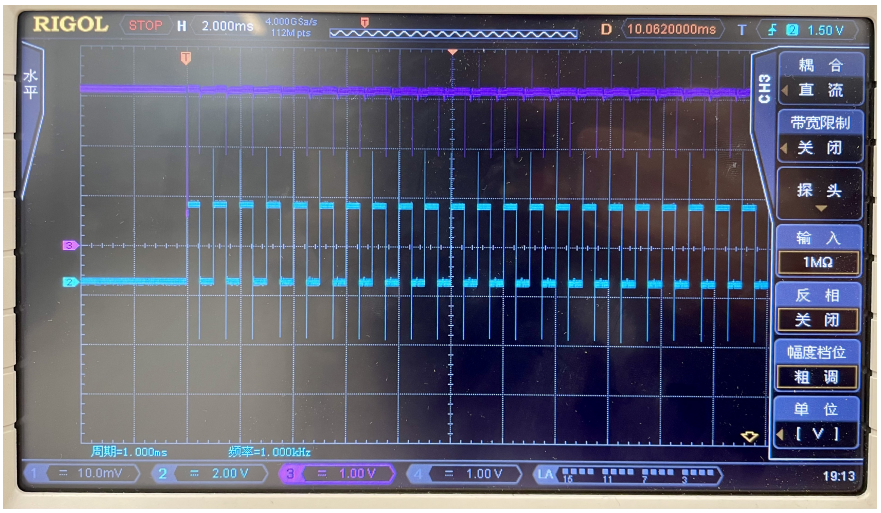

Figure 20: HX711 Data and Clock Frequency

Figure 21: Oscilloscope interface

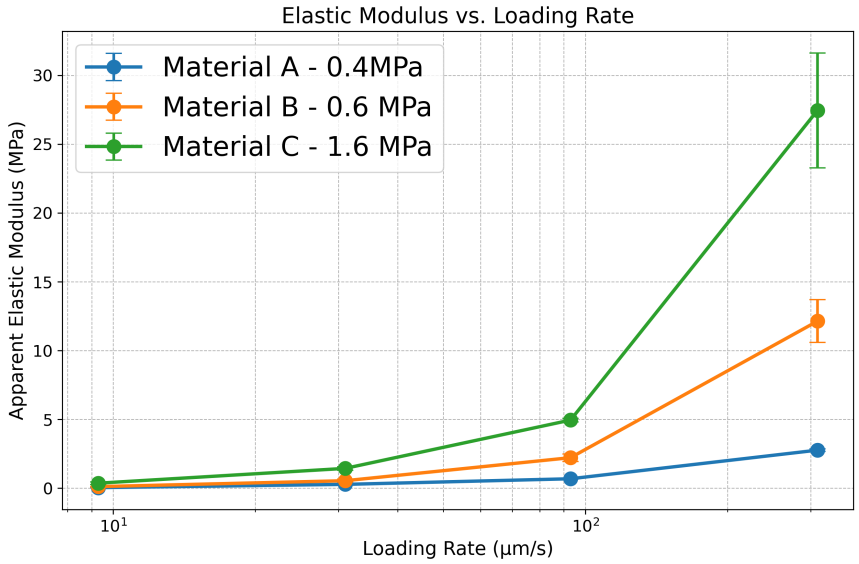

Figure 22: Loading rate experiment

Table 6: Requirements and Verification for Mechanical, Electrical, and Control Modules

Mechanical – Stepper Motor and Screw Coupling	
Requirement	**Verification Method**
Step resolution: 1.0 ± 0.5 μm per step with 1/16 microstepping and 2 mm lead screw.	A. Program motor to move 100 microsteps. B. Measure total displacement via laser sensor. C. Verify average per step is within range.
Mechanical – Cantilever Beam	
Requirement	**Verification Method**
Spring constant k = 10–15× that of target material.	A. Apply known weights (e.g., 10 g). B. Measure deflection using laser sensor. C. Calculate stiffness and check range.
Under 0.1 N force, deflection $\geq$ 0.1 mm to achieve strain $\geq 5 \times 10^{-4}$.	A. Apply force via standard weights. B. Measure tip deflection. C. Calculate strain, verify meets threshold.
Electrical – Analog Interface (Strain Gauge)	
Requirement	**Verification Method**
Balanced Wheatstone bridge when R_x = 220 Ω; V_g reflects resistance change due to bending.	Bridge remains balanced under no strain. Output voltage V_g varies proportionally with resistance change due to bending.

baseline noise should be lower than the resolution of ADC. Excessive noise may introduce extra noise. The noise spectral density should satisfy $S_0 < 100\,\text{nV}/\sqrt{\text{Hz}}$.	Power the bridge using a stable 3.3 V source. Measure the differential output V_g with no applied strain to confirm a balanced state. Using a data acquisition system with sufficient resolution, measure the baseline noise: $$V_{\text{noise, rms}} = \sqrt{\int_{f_{\text{low}}}^{f_{\text{high}}} S_n(f)\, df}$$ Compare the measured baseline noise against the resolution of ADC.
Motor Control – Timer GPIO	
Requirement	**Verification Method**
Output pulses at 500–2000 Hz with $\pm 2\%$ accuracy.	A. Set TIM4 to test frequencies. B. Measure pulse with oscilloscope, compare.
Direction change within 50 ms of command.	A. Send direction switch command. B. Monitor DIR pin response via oscilloscope.
Data Acquisition – HX711 Interface	
Requirement	**Verification Method**
Sample rate $\geq$ 10 Hz, resolution = 24-bit.	A. Set HX711 to 10 Hz mode. B. Log values, confirm timing and resolution.
Peak-to-peak noise under static load $<$10 LSB.	A. Leave cantilever unloaded. B. Record 100 samples, compute noise range.
Application Software – Serial Communication	
Requirement	**Verification Method**
The communication module must achieve bidirectional data transmission at 9600 ±5% baud rate with a maximum data loss rate below 1% during a 60-second continuous test.	A. Connect STM32 and PC via USB-to-UART. B. Transmit a predefined 1KB data packet from PC to STM32 and vice versa at 96000 baud. C. Record the number of successfully received bytes. Compute error rate. Confirm it is less than 1%.

The system must correctly parse and respond to structured command frames of 8 bytes, and update internal status within 100 ms of receiving a valid frame.	A. Use QSerialPort to send valid/invalid 8-byte command frames to STM32. B. Monitor UART response time with oscilloscope or logic analyzer. C. Confirm valid commands are parsed and system reacts (e.g., toggles GPIO) within 100 ms.
Application Software – Data Processing	
Requirement	**Verification Method**
The force conversion algorithm must yield force values with less than ±10% error when compared against standard weights.	A. Apply known calibrated weights to sensor. B. Record strain gauge voltage and compute force using algorithm. C. Compare computed force to ground truth. Verify relative error $<$ 5%.
The Young's modulus estimation model must produce results within ±10% of the known reference values for at least 3 different materials.	A. Run tests on three calibration materials with known Young's modulus. B. Capture force-displacement curve and feed into ML model. C. Compare output modulus with known values. Ensure all deviations less than 10%.
Application Software – User Interface	
Requirement	**Verification Method**
The GUI must refresh the force-displacement graph at a minimum rate of 10 Hz with less than 200 ms latency between data arrival and display.	A. Simulate serial data input at 10 Hz using a test script. B. Use a screen recording tool with timestamp overlay to measure latency. C. Confirm display is updated within 200 ms after each data point.
The user must be able to control motor power and direction through the GUI, with correct serial commands sent upon each interaction.	A. Click each control on the GUI. B. Use a serial monitor to observe outgoing command format. C. Verify commands match specification and motor responds accordingly.

The user must be able to save the data of the F-Z curves after clicking ”Save” and get the result of the elastic modulus calculated from the current curve after clicking ”Calculate”.	A. Click the ”Save” button after generating an F-Z curve. B. Check the file system for a correctly named output file containing time-stamped force and displacement data. C. Click the ”Calculate” button and verify that a Young’s modulus value is displayed, matching the result from an independent offline analysis within 5% error.

Table 7: Mechanical properties of different cantilever samples

Cantilever Design	**Deflection under 0.1N (mm)**	**Elastic Modulus (MPa)**	**Spring Constant (N/m)**
C3	0.31	495.8	267.7
C2	0.03	267.5	1306.3
C1	0.04	766.5	1916.3

Table 8: Direction change time interval for three experiments

Experiment	1	2	3
Get signal from serial port (s)	4.78405932	12.67350790	4.15180078
Direction output changed (s)	4.78406068	12.67350926	4.15180241
Time interval (μs)	1.36	1.36	1.63